Article **Journal Innovative Design**
December, 2022 Vol.6 No.15 1-9

Control based on GLRT algorithm for Unmanned Aerial Vehicle

Control basado en algoritmo GLRT para vehículos aéreos no tripulados

ZAVALA-CONTRERAS, Francisco Javier†, ALAZKI, Hussain, CORTES-VEGA, David* and GOLIKOV, Victor

Universidad Autónoma del Carmen Facultad de ingeniería

ID 1st Author: *Francisco Javier, Zavala-Contreras* /**ORC ID**: 0000-0003-2955-4827, **CVU CONACYT ID**: 1085721

ID 1st Co-author: *Hussain, Alazki* /**ORC ID**: 0000-0002-1960-3624

ID 2nd Co-author: *David, Cortés-Vega* /**ORC ID**: 0000-0002-6209-2081

ID 3rd Co-author: *Victor, Golikov* /**ORC ID**: 0000-0001-7909-9215

DOI: 10.35429/JID.2022.15.6.1.9 Received July 23, 2022; Accepted October 30, 2022

Abstract

This paper proposes the study of a vision-based control scheme for an Unmanned Aerial Vehicle (UAV) for tracking objects floating on the sea surface. The applied vision scheme is based on the generalized likelihood ratio test (GLRT) algorithm. Once the target is detected, its coordinates are computed and used by the UAV control to track the target. The quadrotor mathematical model is developed using the Newton-Euler approach and a PID controller is implemented to track the vector containing the coordinates obtained through the vision scheme. To verify the effectiveness of the proposal, simulation tests are developed in MATLAB/Simulink based on a real video of an objective floating in the sea surface. The obtained results show an appropriate detection and tracking of the objective.

Unmanned Aerial Vehicle, tracking control, GLRT

Resumen

En este artículo se propone el estudio de un esquema de control basado en visión para un Vehículo Aéreo No Tripulado (VANT) para el seguimiento de objetos flotantes sobre la superficie del mar. El esquema de visión aplicado está basado en la prueba de verisimilitud generalizada. Una vez que el objetivo es detectado, sus coordenadas son computarizadas y usadas por el control del VANT para realizar el seguimiento del objetivo. El modelo matemático del cuadrotor es desarrollado usando la aproximación Newton-Euler y el control PID es implementado para seguir el vector que contiene las coordenadas obtenidas a través del esquema de visión. Para verificar la efectividad de la propuesta, pruebas de simulación son desarrolladas en MATLAB/Simulink basándose en un video real de un objetivo flotando sobre la superficie del mar. Los resultados obtenidos muestran una detección y seguimientos apropiados del objetivo.

Vehículos Aéreos No Tripulados, Control de seguimiento, Prueba de verisimilitud generalizada

Citation: ZAVALA-CONTRERAS, Francisco Javier, ALAZKI, Hussain, CORTES-VEGA, David and GOLIKOV, Victor. Control based on GLRT algorithm for Unmanned Aerial Vehicle. Journal Innovative Design. 2022, 6-15: 1-9

*Author's Correspondence (email: dcortes@pampano.unacar.mx)
†Researcher contributing as first author.

© ECORFAN- Taiwan

I. Introduction

The Unmanned Aerial Vehicles (UAV) are versatile tools used to perform several tasks where a human pilot is not desirable. Nowadays, applications in which UAVs are useful are everywhere. In [1], a UAV is used to support the inspection and planning of building construction by giving a better view of the ground conditions, while an obstacle avoidance control was also applied to make the workflow faster. UAVs are also used for data acquisition after a natural disaster, monitoring the development of a city's infrastructure and environmental management as shown in [2]. In [3] a UAV is used for 3D mapping and monitoring tasks of an ecosystem located in Antarctica. To optimize pesticides application over plantations, in [4] a wireless sensor network was installed on a plantation to send relevant information to a UAV that be responsible for controlling the spreading process reducing deviations caused by wind.

Normally when UAVs are used for a specific task, they are controlled remotely by an operator on the ground, or they use sensors to locate themselves such as GPS or an ultrasonic sensor to detect the height at which they fly. However, many times they integrate a camera with which they obtain information to perform mapping or data collection. Some works have been performed where a camera is incorporated in the UAV as a sensor to obtain precise information about its own location, or the location of an object on which trajectory tracking can be performed based on the information collected by the camera. An example of such use of the camera is presented in [5] for the inspection of pipelines carrying gasoline and oil, where a UAV equipped with a non-contact sensor that perform external inspections of the pipes is proposed. The camera is pointing downwards to detect if the pipelines are aligned with the trajectory of the UAV, while a PID controller is responsible for maintaining the angles of the pipe and the desired trajectory.

The algorithms applied to computational vision arise from the necessity of object detection in dangerous environments for humans. One of them is [6], where a vision system is implemented to detect sea mines that were left on the surface of the ocean and avoid them.

In [7] a vision-based control for a UAV monitoring a bridge within an unknown 3D environment is presented, an adaptive nonlinear tracking control law is proposed together with a homography matrix computed from the visual information which allows the effective tracking and depth estimation. The depth estimation is useful for an approximation of the desired distance separating the camera from the target. An application of a computational vision system for a landing maneuver is shown in [8], where the camera detects a landmark by means of contour detection, image thresholding, and other mathematical techniques, obtaining fast, simple, and robust results. In [9] a computer vision system is developed based on an algorithm for landmark detection and tracking, which estimates the UAV motion (position and linear velocity) relative to a landing pad on the ground, the algorithm creates a homography matrix H for each view of the landing pad circles, calculating the height at which the UAV is located.

The work [10] presents an algorithm based on the Generalized Likelihood Ratio Test (GLRT) called Adaptive Subspace Detector (ASD) which aims to detect an object floating in the sea without knowing a priori its size, shape, and position in a sequence of images using optical sensors and infrared devices, the quality of detection is not affected by low contrast or background noise, so it is a viable option for detecting objects. In [11] the ASD and Modified Adaptive Subspace Detector (MASD) algorithms are implemented in some videos collected by a quadrotor with a camera pointing downwards. The videos are analyzed and some parameters such as the window size, the number of harmonics, and the number of frames analyzed are changed to perform a comparison of which algorithm works better under certain conditions.

There are several techniques for the control of UAVs like PID, Feedback linearization, Linear Quadratic Regulation (LQR), Sliding mode, Backstepping among others. The PID has a straightforward structure that is simple to build, offers high performance and a simple parameter's tuning process, is not typically used in underactuated systems but can be adapted to do it, also PID control does not consider the gyroscope effect and ignores air friction too [12].

ISSN-2523-6830
ECORFAN® All rights reserved

The LQR controller can be designed to obtain robust characteristics against disturbances, the stability of the system depends on the correct tuning parameter of the gain matrix K, but more complex calculus must be done. A comparison between PID and LQR is presented in [13], where the ease of implementation of PID controllers stands out over LQR schemes.

Hence this paper proposes the development of a vision-based control system for a quadrotor vehicle using GLRT algorithm to detect an objective floating in the sea surface in every video frame and compute its corresponding trajectory, with a PID controller to track such trajectory.

The remainder of this paper is organized as follows: Section II presents the mathematical model of the quadrotor. Section III presents information related to GLRT vision algorithm operation. Section IV shows a description of the proposed system and section V summarizes the results obtained from the simulation. Finally, section VI presents the conclusions of the work.

II. UAV Mathematical Model

The body of the quadrotor is constituted by 2 bars joined perpendicularly at the center of mass has 4 motors one for each end, the direction of rotation of the motors it's important because if they all spin in the same direction the UAV would start to revolve on *z*-axis that's why the motors must rotate like Figure 1.

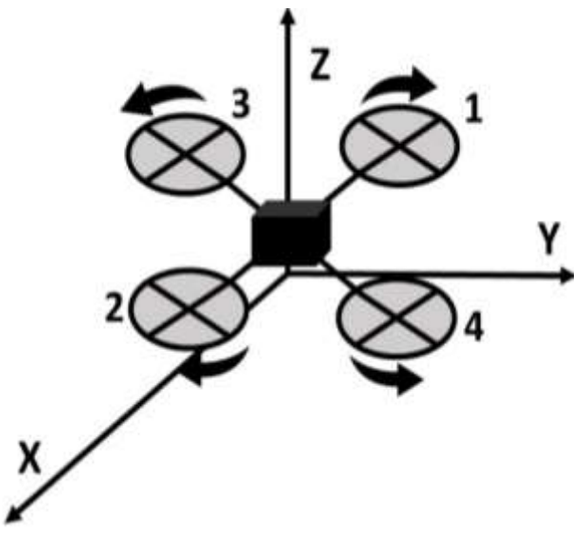

Figure 1 UAV motors alignment

The quadrotor is considered as a solid body and to describe its motion it is necessary to establish 2 reference systems, the first one is fixed to the ground denoted as a vector called J_F for inertial frame equal to:

$$J_F = \{\vec{x}\vec{y}\vec{z}\} \tag{1}$$

The second is associated with the center of mass and is the one that delimits the motion of the quadrotor for the inertial reference system is denoted as F_B:

$$F_B = \{\vec{x}_L\vec{y}_L\vec{z}_L\} \tag{2}$$

From these 2 reference systems it is possible to know the linear and angular position of the UAV. The linear position, the linear velocity and the angular position are described as follows [14]:

$$\xi = [x, y, z]^T \in \mathbb{R}^3 \tag{3}$$

$$\dot{\xi} = v \tag{4}$$

The UAV body can rotate about its center of mass in the 3 axes of the reference frame shown in (2) by the acceleration or deceleration of its four motors, for example, taking into account the organization of the Figure 1 we can say that if we increase the speed of motor 3 and decrease the speed of motor 4 the UAV will rotate on the *x*-axis to the right if we take motor 1 as a front, on the other hand, this rotation can be represented by the rotation matrix on the *x*-axis described below.

$$\begin{bmatrix} x_1 \\ y_1 \\ z_1 \end{bmatrix} = \begin{bmatrix} 1 & 0 & 0 \\ 0 & cos\phi & sin\phi \\ 0 & -sin\phi & cos\phi \end{bmatrix} \begin{bmatrix} x_2 \\ y_2 \\ z_2 \end{bmatrix} \tag{5}$$

where ϕ is a Euler angle for the *x*-axis commonly called Roll.

Furthermore, under the same dynamics, decreasing the power of motor 1 and increasing the power of motor 2 will cause a rotation, but in the *y*-axis with its corresponding rotation matrix:

$$\begin{bmatrix} x_1 \\ y_1 \\ z_1 \end{bmatrix} = \begin{bmatrix} cos\theta & 0 & sin\theta \\ 0 & 1 & 0 \\ -sin\theta & 0 & cos\theta \end{bmatrix} \begin{bmatrix} x_2 \\ y_2 \\ z_2 \end{bmatrix} \tag{6}$$

where θ is Euler angle for the *y*-axis called Pitch

ECORFAN® All rights reserved

In this case, increasing the power of motors 1 and 2 would cause rotation in the UAV over the *z*-axis clockwise, otherwise, increasing the power of motors 3 and 4 would cause rotation in the UAV counterclockwise over the *z*-axis, the rotation matrix is shown below:

$$\begin{bmatrix} x_1 \\ y_1 \\ z_1 \end{bmatrix} = \begin{bmatrix} cos\psi & -sin\psi & 0 \\ sin\psi & cos\psi & 0 \\ 0 & 0 & 1 \end{bmatrix} \begin{bmatrix} x_2 \\ y_2 \\ z_2 \end{bmatrix} \quad (7)$$

where ψ is Euler angle for the *z*-axis called Yaw. By multiplying the three matrices it is possible to constitute the rotation matrix of F_B that will give the position of the rigid body for the inertial frame this matrix it is called the cosine matrix[15]:

$$R_I = \begin{pmatrix} C\psi C\theta & C\psi S\phi S\theta - C\phi S\psi & S\phi S\psi + C\phi C\psi S\theta \\ C\theta S\psi & C\phi C\psi + S\phi S\psi S\theta & C\phi S\psi S\theta - C\psi S\phi \\ -S\theta & C\theta S\phi & C\phi C\theta \end{pmatrix} \quad (8)$$

where $C(*)$ stands for cosine and $S(*)$ for sinus. The dynamics of the system is divided in 2 main parts the translational and the orientation, where the first 3 equations are fully based on Newton's second law and describe translational motion based on the direction cosine matrix and multiplies the force shown below:

$$m \begin{bmatrix} \ddot{x} \\ \ddot{y} \\ \ddot{z} \end{bmatrix} + mg \begin{bmatrix} 0 \\ 0 \\ 1 \end{bmatrix} = R_I F \quad (9)$$

Where m is mass and g is the gravity form this multiplication is derived from the next three equations describing the lineal movement of the UAV:

$$\ddot{x} = \frac{1}{m}(\cos\psi sin\theta cos\phi + \sin\psi \sin\phi)\frac{U_1}{m} \quad (10)$$

$$\ddot{y} = \frac{1}{m}(\sin\psi sin\theta cos\phi + \cos\psi \sin\phi)\frac{U_1}{m} \quad (11)$$

$$\ddot{z} = -g + \frac{1}{m}(cos\ \theta cos\phi)\frac{U_1}{m} \quad (12)$$

where U_1 is the principal control signal of the 4 motors.

On the other hand, the second part of the model is the orientational system with three equations describing the angular movement of the UAV. The angular position vector and the angular velocity vector are described by:

$$\eta = [\phi, \theta, \psi]^T \quad (13)$$

$$\omega = [p\ q\ r]^T \quad (14)$$

where η is the angular position vector, $p\ q$ and r the angular velocity of the UAV for the *x*, *y* and *z*-axis The total kinetic energy of the system as a function of generalized coordinates of η is expressed as:

$$E_{cR} = \frac{1}{2}\dot{\eta}^T J(\eta)\dot{\eta} \quad (15)$$

where $J(\eta)$ is the Jacobian matrix defined as:

$$J(\eta) = W_\eta^T I W_\eta \quad (16)$$

the relationship between ω and $\dot{\eta}$ is given through the Jacobian W_η which is represented by the matrix

$$W_\eta = \begin{bmatrix} 1 & 0 & -sin\theta \\ 0 & cos\phi & cos\theta sin\phi \\ 0 & -sin\phi & cos\theta cos\phi \end{bmatrix} \quad (17)$$

and the inertia matrix *I*

$$I = \begin{bmatrix} I_{xx} & 0 & 0 \\ 0 & I_{yy} & 0 \\ 0 & 0 & I_{zz} \end{bmatrix} \quad (18)$$

performing the multiplication of all the matrices, the matrix result is:

$$J_\eta = \begin{bmatrix} I_{xx} & 0 & -I_{xx}S\theta \\ 0 & I_{yy} & (I_{yy} - I_{xx})C\phi S\phi C\theta \\ -I_{xx}S\theta & (I_{yy} - I_{xx})C\phi S\phi C\theta & I_{xx}S^2\theta + I_{yy}S^2\phi C^2\theta + I_{zz}C^2\phi C^2\theta \end{bmatrix} \quad (19)$$

the rotational equations for the three axes are as follows:

$$\ddot{\phi} = \frac{(I_{xx}+I_{yy}-I_{zz})}{I_{xx}}\dot{\psi}\dot{\theta} + \frac{\tau_\phi}{I_{xx}} \quad (20)$$

$$\ddot{\theta} = \frac{(-I_{xx}-I_{yy}+I_{zz})}{I_{yy}}\dot{\psi}\dot{\phi} + \frac{\tau_\theta}{I_{yy}} \quad (21)$$

$$\ddot{\psi} = \frac{(I_{xx}-I_{yy}+I_{zz})}{I_{zz}}\dot{\phi}\dot{\theta} + \frac{\tau_\psi}{I_{zz}} \quad (22)$$

where I_{xx}, I_{yy} and I_{zz} are the moments of inertia in the *x*, *y*, and *z* axes.

ECORFAN® All rights reserved

III. GLRT algorithm

GLRT allows object detection even when the size, shape, and position are unknown using a sequence of images as input data. It is used like a universal detector for detection problems. There are two options for this kind of detector; if the target is present during a scan, it will return the signal target plus the signal from the background clutter; otherwise, if no target is present, it will return exclusively the background clutter. The basic premises for modeling a sequence of pixels are: 1) the background consists of several oscillating elements and 2) the target oscillates as a solid element [12]. It uses video spatial-temporal patches, called bricks, to determine whether the observed brick contains a target in the presence of a random background. A hypothesis test is made to distinguish a pixel with the signal of the target-plus noise (H_1) these pixels contain the target signal plus channel noise from the others who contain the background clutter plus channel noise.(H_0).Under H_0 we have:

$$x_j = \sigma_{0,j} n_j \tag{23}$$

where x_j are a real pixel-vectors, n_j is the noise pixel-vector and $\sigma_{0,j}$ is the variance of the background plus channel noise. Under H_1 is the signal plus background plus channel noise hypothesis is:

$$x_j = s_j + \sigma_{1,j} n_j \tag{24}$$

Where $s_j = H\theta_j$ is the deterministic signal of interest that belongs to a known subspace, H is an orthogonal target Vandermonde matrix:

$$H = \begin{bmatrix} 1 & 1 & \dots & 1 \\ Z_1 & Z_2 & \dots & Z_p \\ \vdots & \vdots & \dots & \vdots \\ Z_1^{K-1} & Z_2^{K-1} & \dots & Z_p^{K-1} \end{bmatrix} \tag{25}$$

Hence it is considered the problem of detecting an optical target in N digital images, assuming the target may be present completely or partially in the brick with size L of pixel vectors, Let $j = 1, \dots, U$ be a subset of integers indexing the pixel vectors (U is unknown) which may contain an unknown object under the H_1 hypothesis and $j = U + 1, \dots, L$ is the subset of the pixel-vectors, which do not contain the object under the H_1.

The secondary dataset consists of GL pixel vector$x_j, N \times 1, j = L + 1,2, \dots, (G + 1)L$ which are assumed to have the background clutter and white channel noise components only.

Then, the hypotheses can be expressed as:

$$\begin{cases} H_0: x_j = c_j + n_j, j = 1,2, \dots, (G+1)L \\ H_1: \begin{cases} x_j = s_j + n_j, j = 1, \dots, U \\ x_j = c_j + n_j, j = U+1, \dots, (G+1)L \end{cases} \end{cases} \tag{26}$$

IV. Vision-based control scheme

The proposed vision-based control scheme is illustrated in the block diagram in Figure 2.

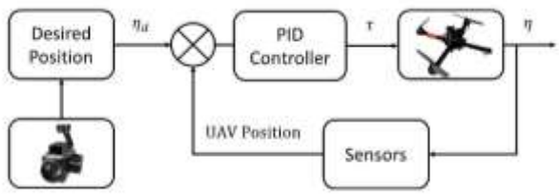

Figure 2 Block diagram of the proposed scheme

The PID-based control scheme uses 4 references to control the 6 degrees of freedom of the UAV movement as previously defined, 6 equations were developed to describes those movements.

The mathematical model is inserted in Simulink allowing the simulation of the system, the references are, the linear displacement in the *z*-axis, in which all the motors are used at the same time to lift the UAV body, and the control of the rotations in the 3 axes of the angular displacement on the body coordinate system. It is through these rotations that indirectly the body can move along the *x* and *y* axes linearly.

The PID control can follow trajectories in the *xy* plane under the consideration of a fixed height, so the *xy* plane can be related to the input images that also have two dimensions (height and width). The parameters used in the simulation for the model of the considered quadrotor are shown in Table 1.

ISSN-2523-6830
ECORFAN® All rights reserved

Parameter	Symbol	Value
Gravity	g	9.81 m/s^2
Mass	m	0.468 kg
Length of arm	l	0.225 m
Drag constant	d	2.98e-6 $N*m*s^2$
Thrust constant	b	2.930e-6 N*s^2
Rotor inertia	J_r	3.335e-5 $kg*m^2$
Inertia in *x*-axis	I_{xx}	4.856e-3 $kg*m^2$
Inertia in *y*-axis	I_{yy}	4.856e-3 $kg*m^2$
Inertia in *z*-axis	I_{zz}	8.801e-3 $kg*m^2$

Table 1 Values form the mathematical model

The vision algorithm uses images obtained from a camera mounted inside the body of the UAV. After obtaining these images analyzes a set of these, within each image there are two types of frame, a detection frame and a frame that is responsible for collecting data to generate the threshold that determines whether the target is present or not, the frame that generates the threshold is a square of 10 pixels by 10 pixels, while the detection region is selected as a frame where the object is intended to be detect, a sample of 50 images where the target was detected in various positions was taken.

As the image is an array of pixels in two dimensions, the pixels can be taken as units of a cartesian plane and the pixels in which the target was detected become points that can be located with 2 numbers expressed in coordinates, these coordinates have their point of origin in the lower left corner. Once the coordinates of the points along the 50 images are collected, it is possible to transform these data into elements of a vector of positions that will generate a trajectory. Such trajectory is used as the reference to be tracked by the quadrotor using a PID-based control scheme.

V- Results

In order to validate the viability of the proposal a simulation test has been developed in Matlab/Simulink. The objective detection and trajectory generation are performed on a video taken from a quadrotor with a mounted camera. This video shows a person, which is the objective to detect, swimming in the sea's surface with some waves as illustrated in Figure 3.

Figure 3 Objective in one frame of the video

Once the objective is detected the algorithm computes its trajectories and send them to the quadrotor to perform its tracking. The tracking process is based on PD controllers in cascade for the *x* and *y* axes, while a direct loop is used for the *z* axis like it's shown in the Figure 4.

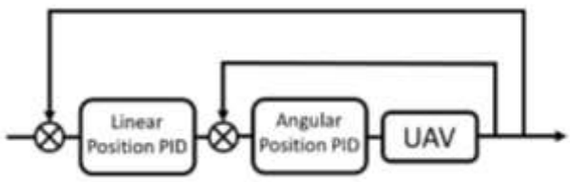

Figure 4 Controller PD in cascade

The corresponding parameters of these controllers are shown in Table 2.

Controller	P	I	D
Linear Position loop (*x*-axis)	1	/	0.5
Linear Position loop (*y*-axis)	1	/	0.5
Linear Position loop (*z*-axis)	5	/	8
Angular Position loop (*x*-axis)	1	10	1
Angular Position loop (*y*-axis)	1	10	1

Table 2 PID controller parameters

The objective of the proposed vision-based control scheme is to keep this target within the camera range, ensuring that the target is under the UAV. The trajectories obtained from the vision algorithm were introduced as the desired reference positions into the mathematic model of the quadrotor to perform the trajectory tracking stage.

ISSN-2523-6830
ECORFAN® All rights reserved

The height at which the video was taken is approximately 10 meters, so this is the desired value used for the *z*-axis. Since height is supposed constant the control objective is to maintain this value at every instant which is depicted in Figure 5.

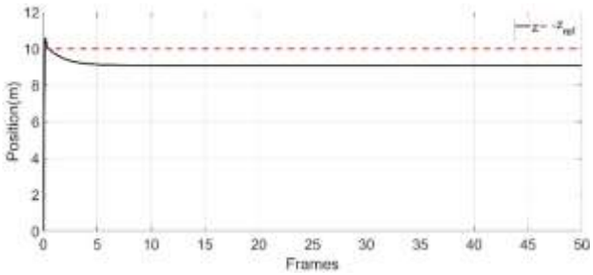

Figure 5 Desired and actual trajectories in *z*-axis

In another hand for the *x*-axis the path it is according to the coordinate of the image width this parameter allows to the PID controller to follow the target across all the *xy* plane to keep it in the center of the image. In the Figure 5 the location of the target and the position of the UAV are shown, in the beginning they are separated but the PID controller acts to align the UAV's position with that of the detected object.

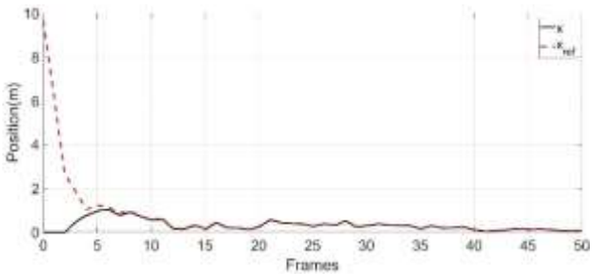

Figure 6 Desired and actual trajectories in *x*-axis

The desired and actual trajectories for the *y*-axis are shown in Figure 7. The object has low movement in this axis, so the trajectory shows small changes which are tracked with enough accuracy by the controller.

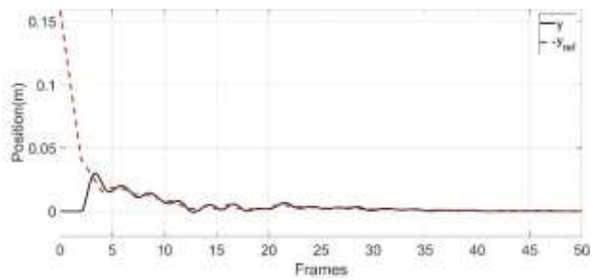

Figure 7 Desired and actual trajectories in *y*-axis

The tracking error for all axes is presented in Figure 8, where can be observed that the desired trajectory for the *x* and *y* axes is properly tracked with low error values. On the other hand, the controller for *z*-axis shows a greater steady state error which can be improved with a better tuning of controller gains.

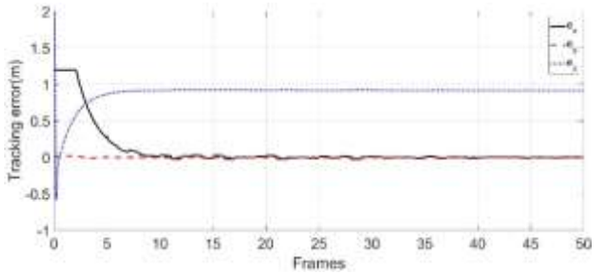

Figure 8 Tracking error (*x*-*y*-*z*-axis)

VI. Conclusions

This work presented the development of a vision-based control scheme for tracking objectives with a quadrotor equipped with a video camera. The GLRT algorithm is used to fulfill the detection task due to its robust features which allows the detection under unknown shape, size and position of the target. Once the detection is performed, the objective coordinates are computed to generate a trajectory to be tracked by a control scheme which ensures that the objective is inside the camera range. A PID control scheme is selected due to its simple tuning and implementation.

The results obtained show a good behavior of the detector, despite the constant oscillation generated by the sea waves, it managed to capture with sufficient accuracy the target within the image allowing the generation of the objective trajectory. The PID control was able to maintain an appropriated tracking of the given coordinates both in the *x* and *y* axis, however, the desired height was not reached remaining at 9 meters when the reference is 10. As future work an improvement in the control of the UAV can be done to maintain a correct altitude, as well as a real time application of the system to be tested in a disturbed environment.

Acknowledgements

To CONACYT and Universidad Autónoma del Carmen (UNACAR)

ISSN-2523-6830
ECORFAN® All rights reserved

Funding

This work has been funded by CONACYT [1085721] and Universidad Autónoma del Carmen (UNACAR) [153129]

References

[1] Freimuth, H., & König, M. (2018). Planning and executing construction inspections with unmanned aerial vehicles. Automation in Construction, 96, 540-553. https://doi.org/10.1016/j.autcon.2018.10.016

[2] Ezequiel, C. A. F., Cua, M., Libatique, N. C., Tangonan, G. L., Alampay, R., Labuguen, R. T., ... & Palma, B. (2014, May). UAV aerial imaging applications for post-disaster assessment, environmental management and infrastructure development. In 2014 International Conference on Unmanned Aircraft Systems (ICUAS) (pp. 274-283). IEEE. https://doi.org/10.1109/ICUAS.2014.6842266

[3] Lucieer, A., Turner, D., King, D. H., & Robinson, S. A. (2014). Using an Unmanned Aerial Vehicle (UAV) to capture micro-topography of Antarctic moss beds. International journal of applied earth observation and geoinformation, 27, 53-62. https://doi.org/10.1016/j.jag.2013.05.011

[4] Faiçal, B. S., Pessin, G., Geraldo Filho, P. R., Carvalho, A. C., Furquim, G., & Ueyama, J. (2014, November). Fine-tuning of UAV control rules for spraying pesticides on crop fields. In 2014 IEEE 26th International Conference on Tools with Artificial Intelligence (pp. 527-533). IEEE. https://doi.org/10.1109/ICTAI.2014.85

[5] Shukla, A., Xiaoqian, H., & Karki, H. (2016, October). Autonomous tracking of oil and gas pipelines by an unmanned aerial vehicle. In 2016 IEEE 59th International Midwest Symposium on Circuits and Systems (MWSCAS) (pp. 1-4). IEEE. https://doi.org/10.1109/MWSCAS.2016.7870114

[6] Borghgraef, A., Barnich, O., Lapierre, F., Van Droogenbroeck, M., Philips, W., & Acheroy, M. (2010). An evaluation of pixel-based methods for the detection of floating objects on the sea surface. EURASIP Journal on Advances in Signal Processing, 2010, 1-11. https://doi.org/10.1155/2010/978451

[7] Metni, N., Hamel, T., & Derkx, F. (2005, December). Visual tracking control of aerial robotic systems with adaptive depth estimation. In Proceedings of the 44th IEEE Conference on Decision and Control (pp. 6078-6084). IEEE. https://doi.org/10.1109/CDC.2005.1583134

[8] Vidal, V. F., Honório, L. M., Santos, M. F., Silva, M. F., Cerqueira, A. S., & Oliveira, E. J. (2017, May). UAV vision aided positioning system for location and landing. In 2017 18th international carpathian control conference (ICCC) (pp. 228-233). IEEE. https://doi.org/10.1109/CarpathianCC.2017.7970402

[9] Carrillo, L. R. G., Rondon, E., Sanchez, A., Dzul, A., & Lozano, R. (2010). Position control of a quad-rotor UAV using vision. IFAC Proceedings Volumes, 43(15), 31-36. https://doi.org/10.3182/20100906-5-JP-2022.00007

[10] Rodriguez-Blanco, M., & Golikov, V. (2016). Multiframe GLRT-based adaptive detection of multipixel targets on a sea surface. IEEE Journal of Selected Topics in Applied Earth Observations and Remote Sensing, 9(12), 5506-5512. https://doi.org/10.1109/JSTARS.2016.2582383

[11] Torres, L. S., Golikov, V., Zhilyakov, E., & Alazki, H. (2019, November). Target Detection On The Sea Surface Using a Quadrotor with a Video Camara. In 2019 IEEE International Autumn Meeting on Power, Electronics and Computing (ROPEC) (pp. 1-6). IEEE. https://doi.org/10.1109/ROPEC48299.2019.9057083

[12] Salih, A. L., Moghavvemi, M., Mohamed, H. A., & Gaeid, K. S. (2010). Flight PID controller design for a UAV quadrotor. Scientific research and essays, 5(23), 3660-3667. https://doi.org/10.5897/SRE.9000032

[13] Bouabdallah, S., Noth, A., & Siegwart, R. (2004, September). PID vs LQ control techniques applied to an indoor micro quadrotor. In 2004 IEEE/RSJ International Conference on Intelligent Robots and Systems (IROS)(IEEE Cat. No. 04CH37566) (Vol. 3, pp. 2451-2456). IEEE. https://doi.org/10.1109/IROS.2004.1389776

ECORFAN® All rights reserved

[14] Castillo, P., García, P., Lozano, R., & Albertos, P. (2007). Modelado y estabilización de un helicóptero con cuatro rotores. Revista Iberoamericana de Automática e Informática Industrial RIAI, 4(1), 41-57. https://doi.org/10.1016/S1697-7912(07)70191-7

[15] Chen, Y., He, Y., & Zhou, M. (2013). Modeling and control of a quadrotor helicopter system under impact of wind field. Research Journal of Applied Sciences, Engineering and Technology, 6(17), 3214-3221. http://dx.doi.org/10.19026/rjaset.6.3626

ISSN-2523-6830
ECORFAN® All rights reserved